SUPPORTING INFORMATION

Chinese Journal of Structural Chemistry

Ultrathin $ZnIn_2S_4$ Nanosheets Supported Metallic Ni_3FeN for Photocatalytic Coupled Selective Alcohol Oxidation and H_2 Evolution

Mengqing Li[1], Weiliang Qi[2], Jiuyang Yu[2], Lijuan Shen[1], Xuhui Yang[1], Siqi Liu[2]* and Min-Quan Yang[1]*

[1]*College of Environmental Science and Engineering, Fujian Key Laboratory of Pollution Control & Resource Reuse, Fujian Normal University, Fuzhou 350007, China*

[2]*School of Environmental Science and Technology, Dalian University of Technology, Dalian 116024, China*

Corresponding authors. Emails: yangmq@fjnu.edu.cn and liusiqi@dlut.edu.cn

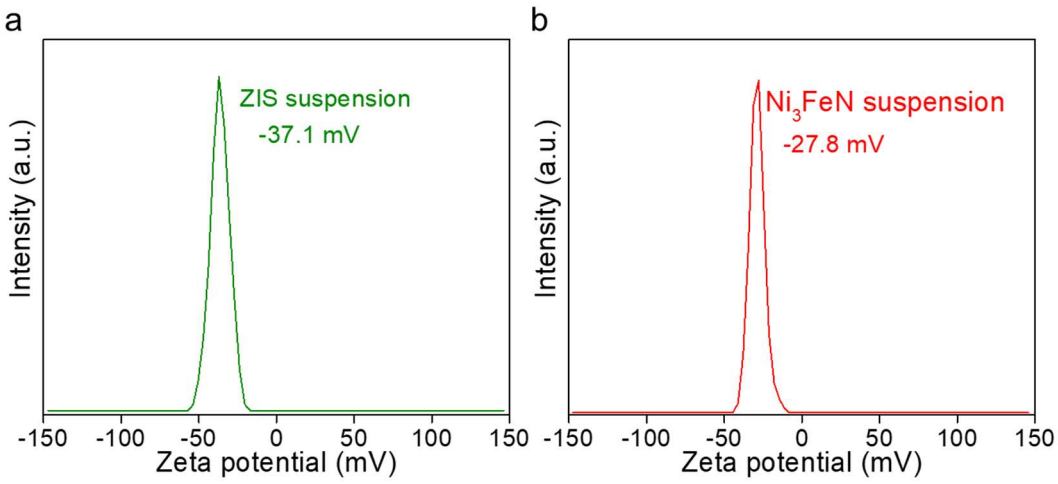

Figure S1. Zeta potential of ZIS and Ni_3FeN suspension dispersed in DI water.

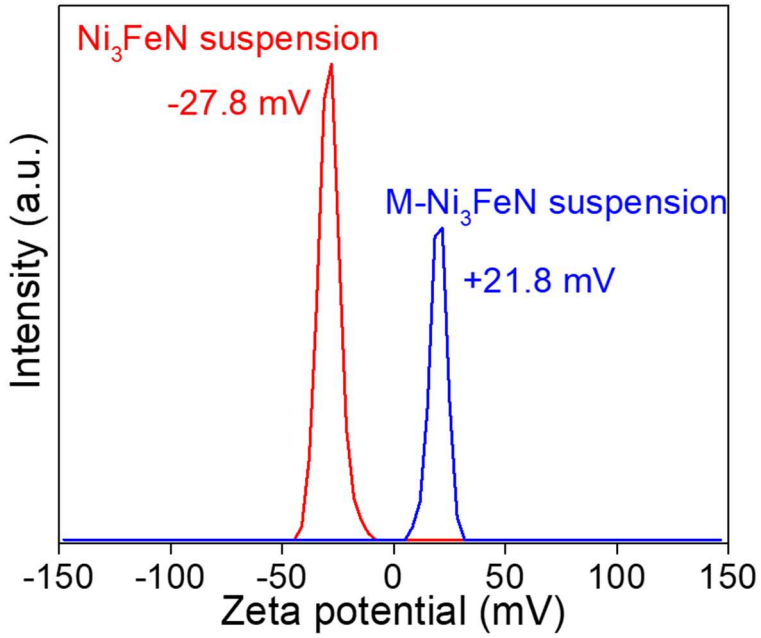

Figure S2. Zeta potential of Ni_3FeN suspension dispersed in DI water before and after surfactant APTES modification.

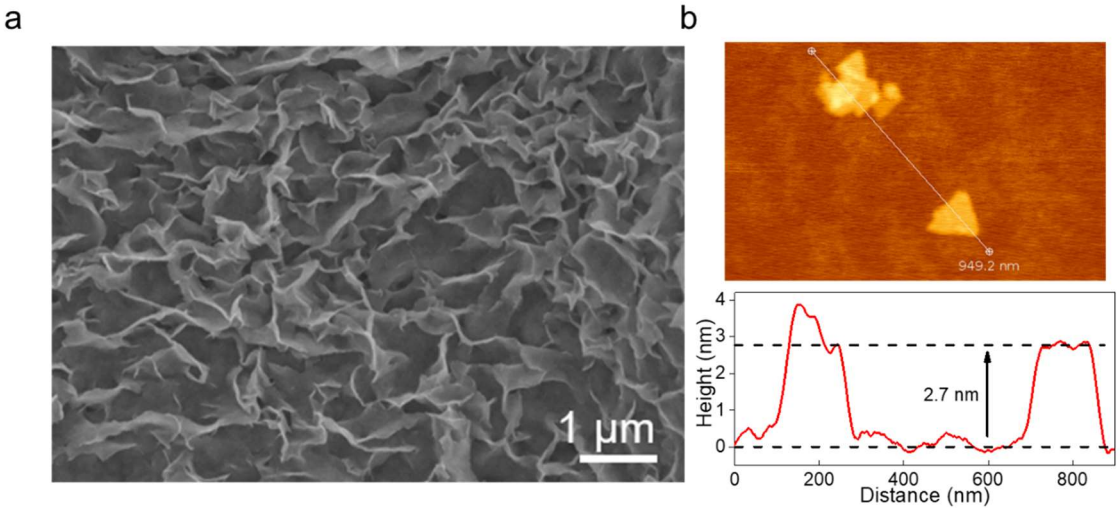

Figure S3. (a) SEM image and (b) AFM image of ZIS.

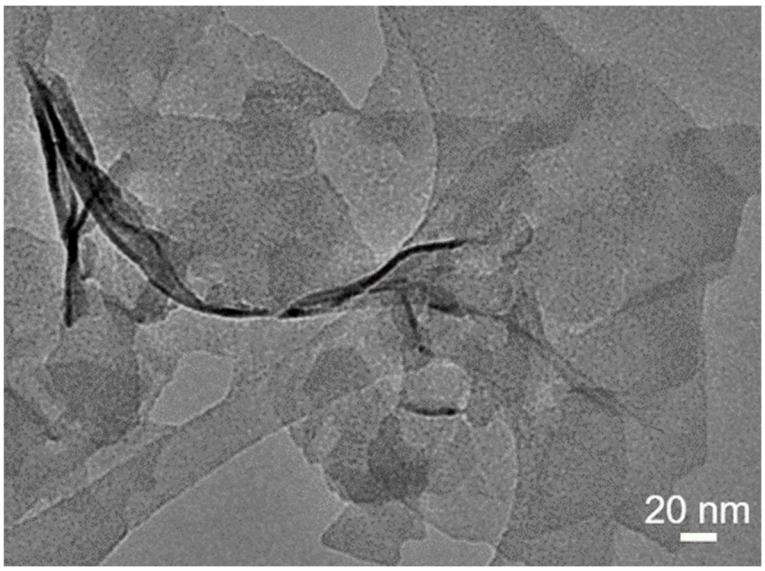

Figure S4. TEM image of bare ZIS.

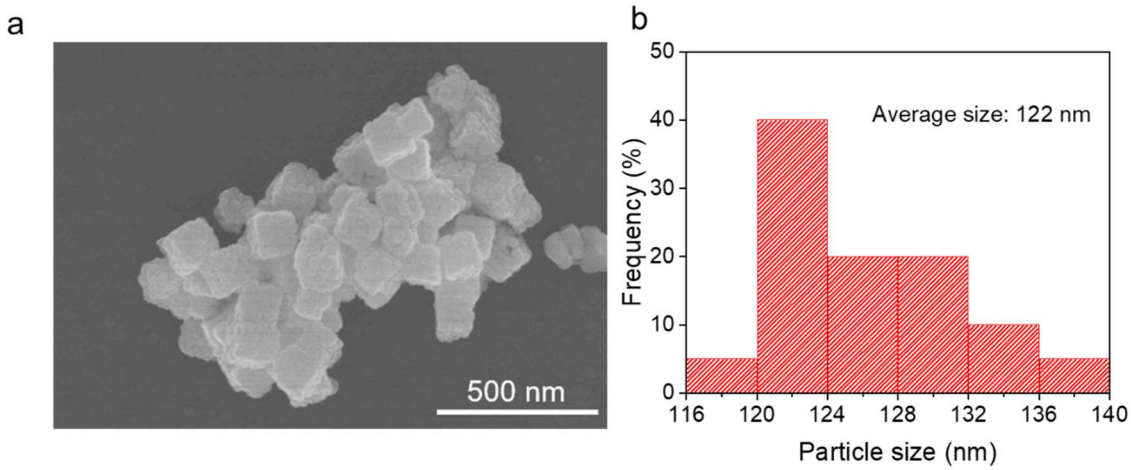

Figure S5. (a) SEM image and (b) the statistic histogram of the size distribution of Ni_3FeN NPs.

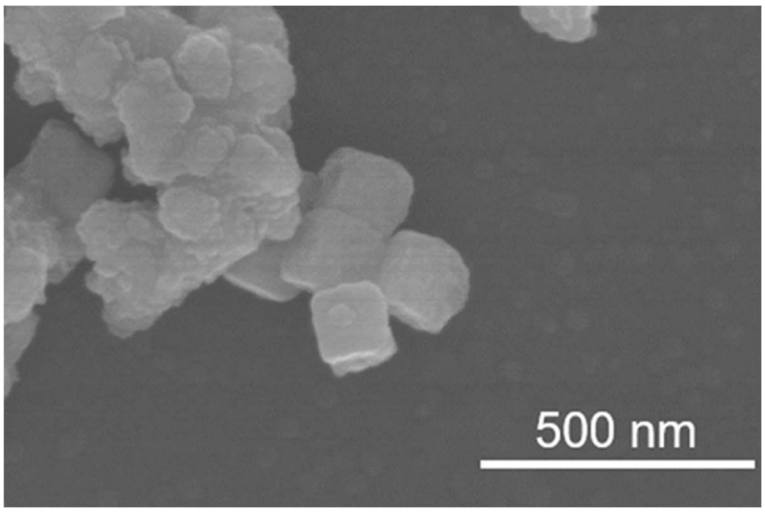

Figure S6. SEM of Ni_3FeN after APTES modification.

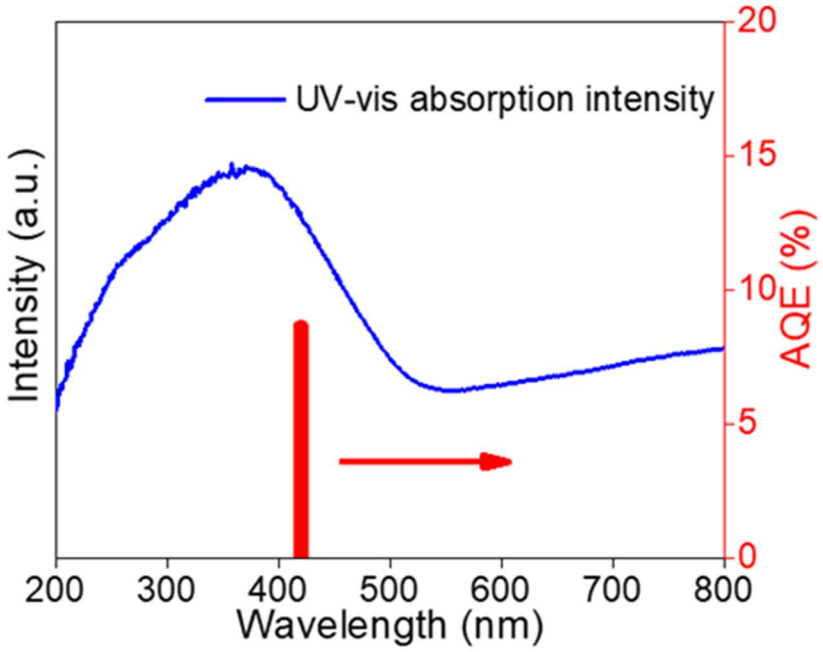

Figure S7. The apparent quantum efficiency at 420 nm of ZIS/1.5% M-Ni_3FeN composite.

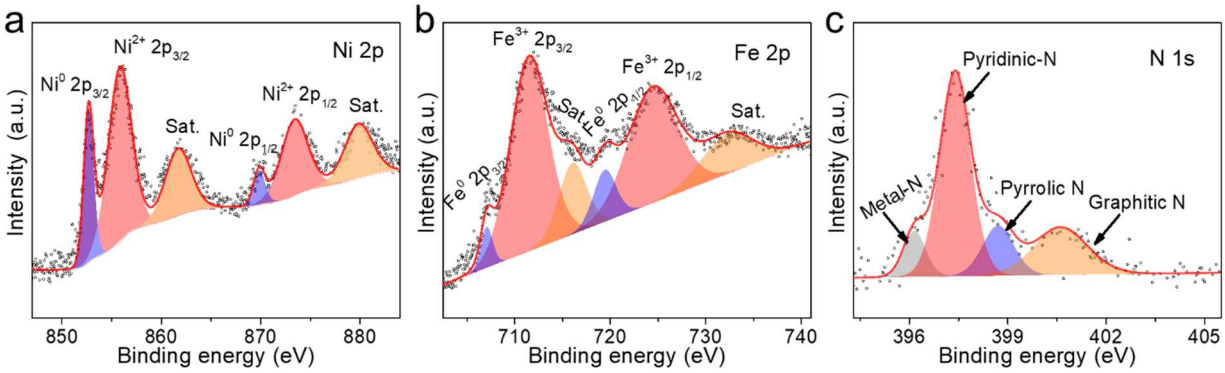

Figure S8. XPS spectra of (a) Ni 2p, (b) Fe 2p and (c) N 1s of ZIS/M-Ni_3FeN composite after the photoactivity test.

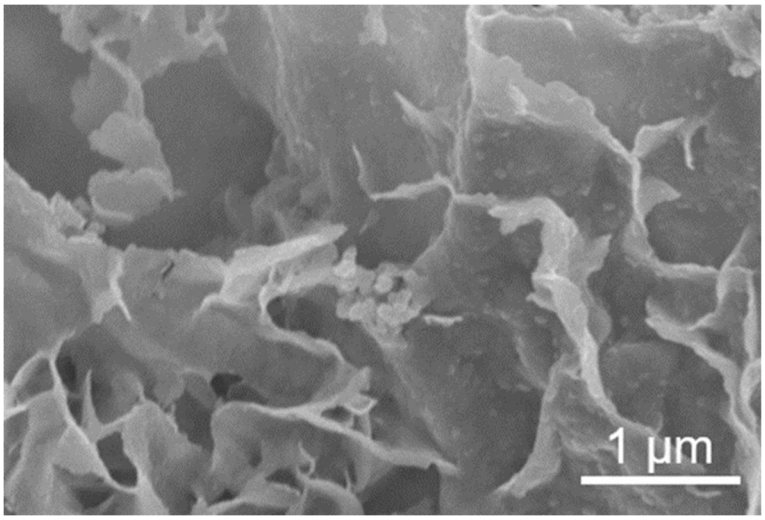

Figure S9. SEM image of ZIS/M-Ni_3FeN composite after the photoactivity test.

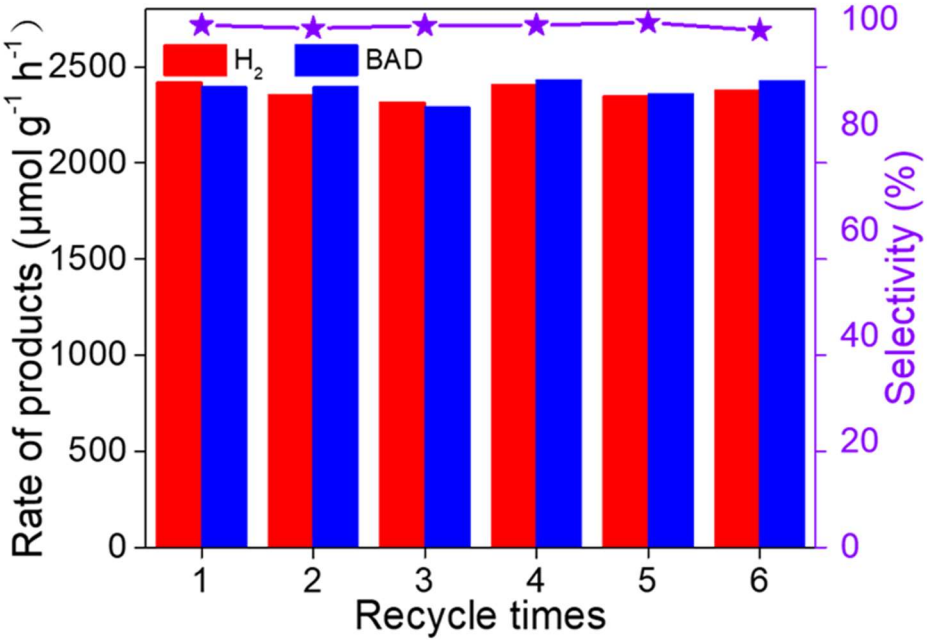

Figure S10. Photocatalytic cyclic test of anaerobic oxidation of benzyl alcohol to produce benzaldehyde and H_2 over ZIS/1.5% M-Ni_3FeN composite.

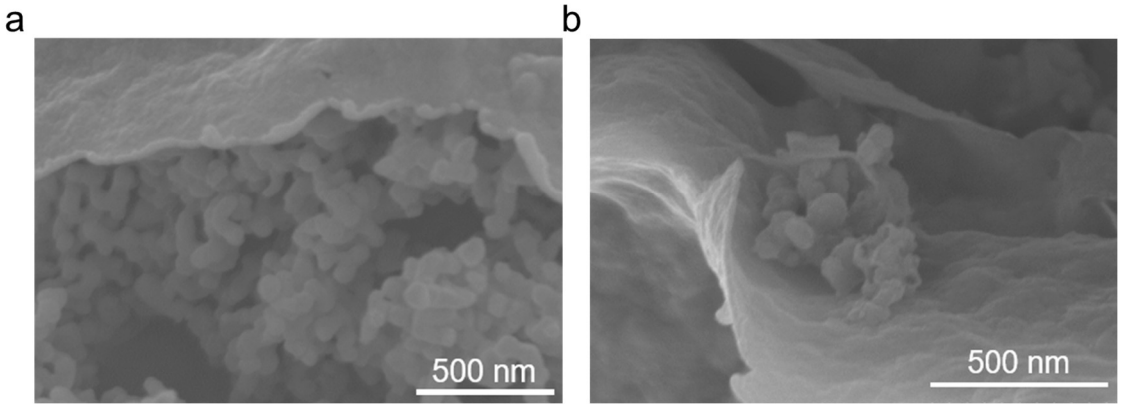

Figure S11. SEM image of ZIS/P-Ni_3FeN composite.

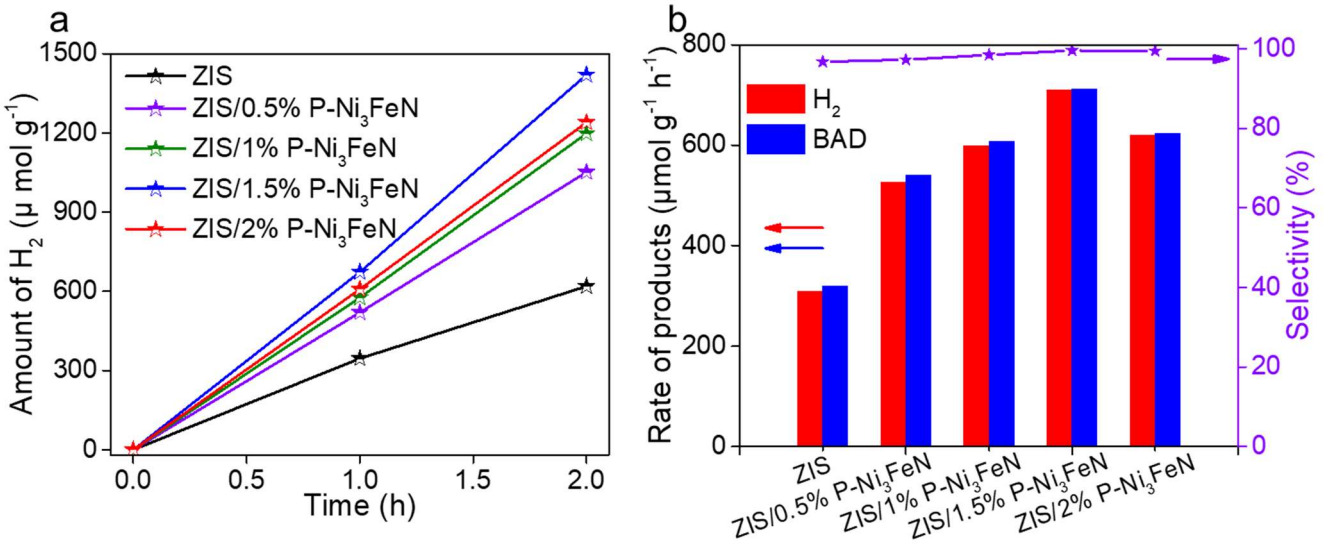

Figure S12. Photocatalytic activity for selective BA oxidation integrated with H_2 evolution over ZIS and ZIS/x% P-Ni_3FeN hybrids.

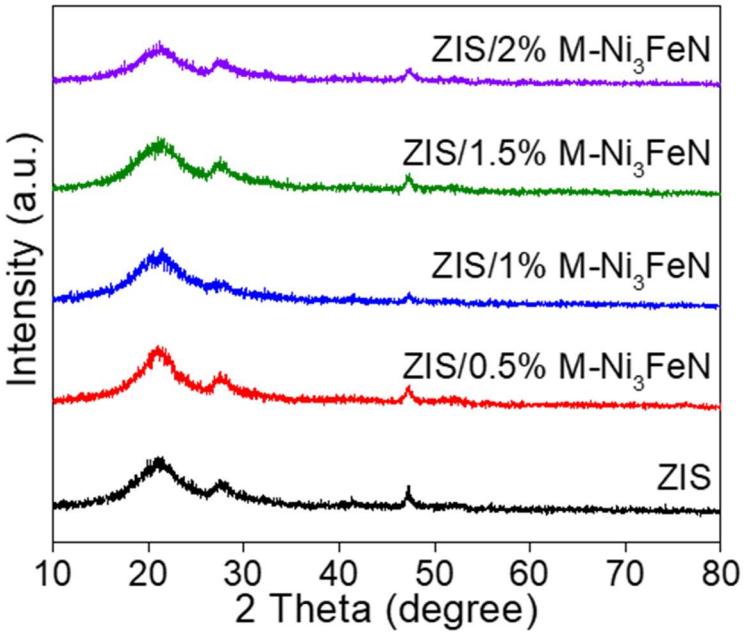

Figure S13. XRD patterns of ZIS and ZIS/x% M-Ni_3FeN hybrids.

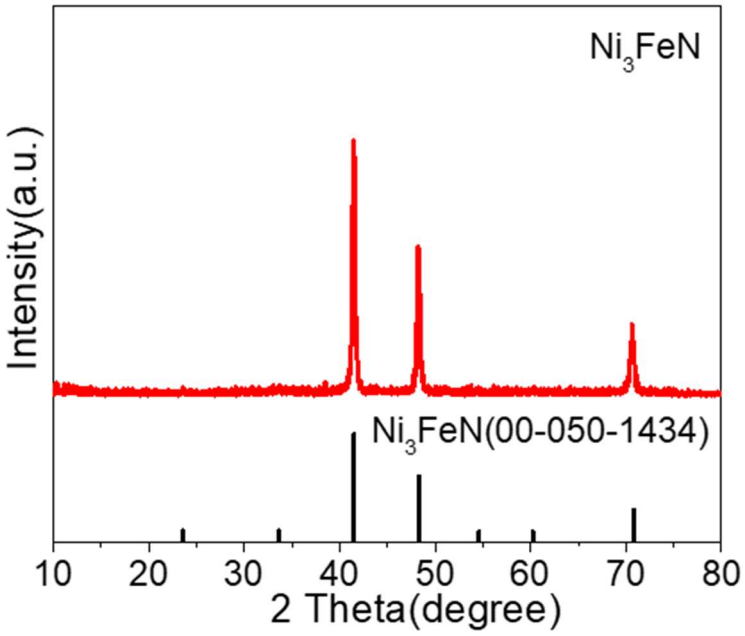

Figure S14. XRD pattern of Ni_3FeN NPs.

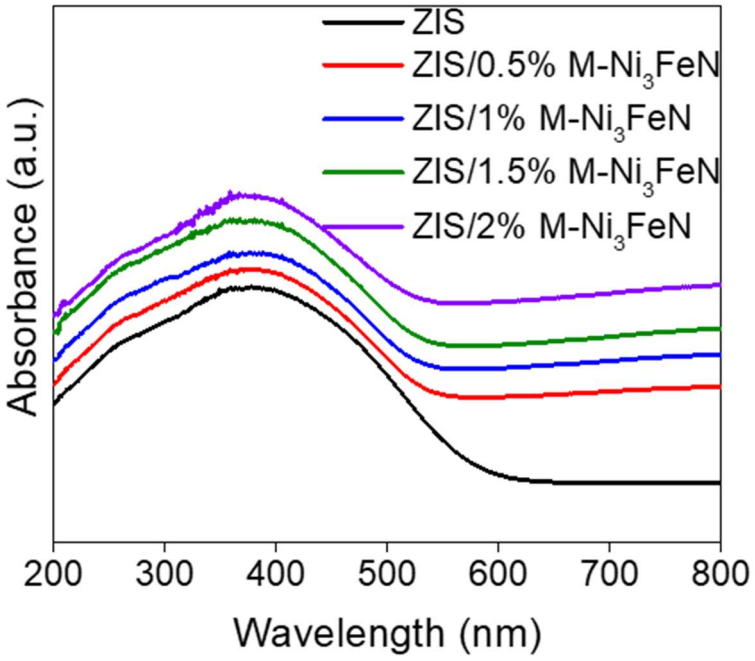

Figure S15. DRS spectra of ZIS and ZIS/x% M-Ni_3FeN hybrids.

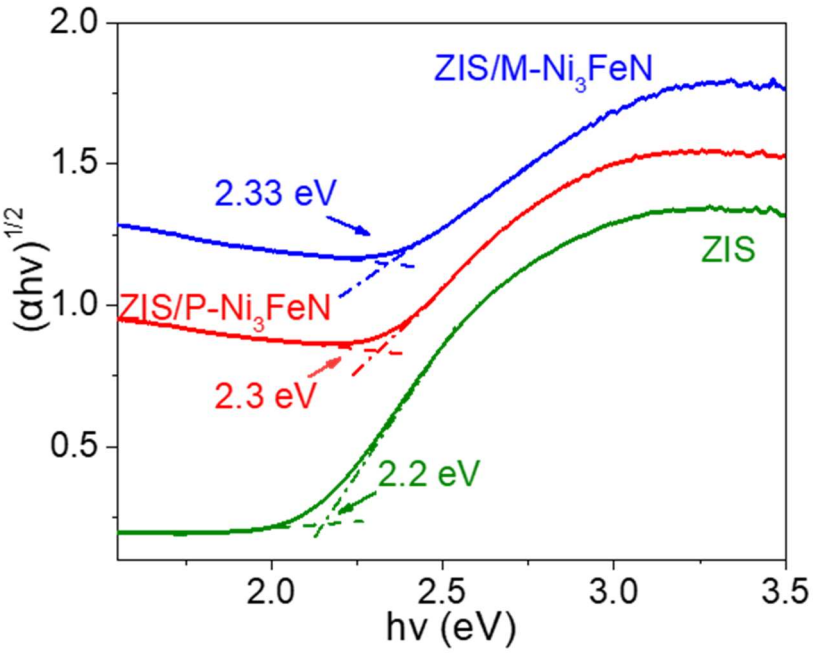

Figure S16. Tauc Plots of the $(\alpha hv)^{1/2}$ vs. photon energy (hv) of bare ZIS, ZIS/P-Ni_3FeN and ZIS/M-Ni_3FeN.

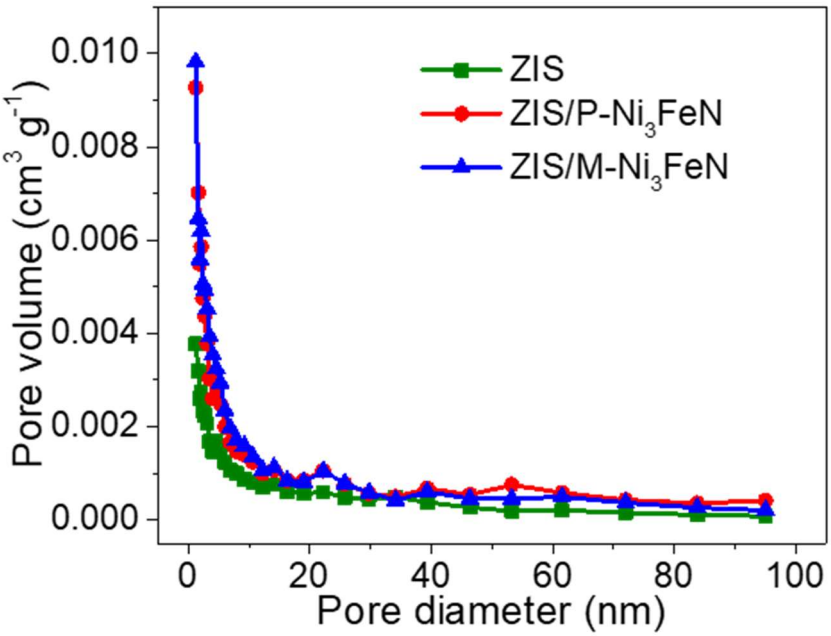

Figure S17. BJH pore size distributions of bare ZIS, ZIS/P-Ni_3FeN and ZIS/M-Ni_3FeN.

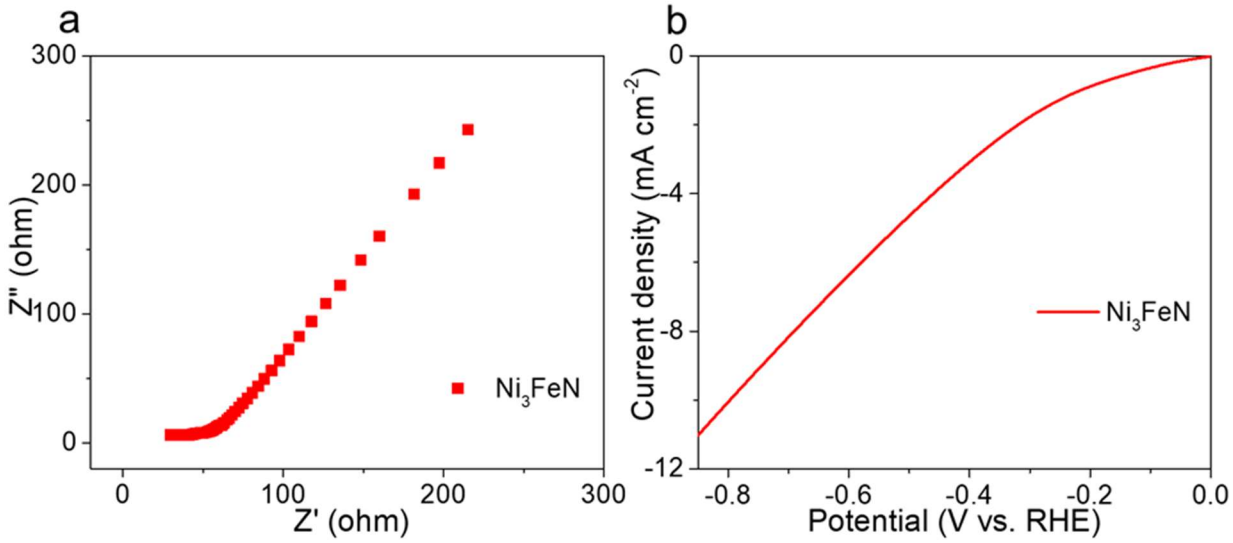

Figure S18. EIS Nyquist plot and LSV curve of Ni_3FeN.

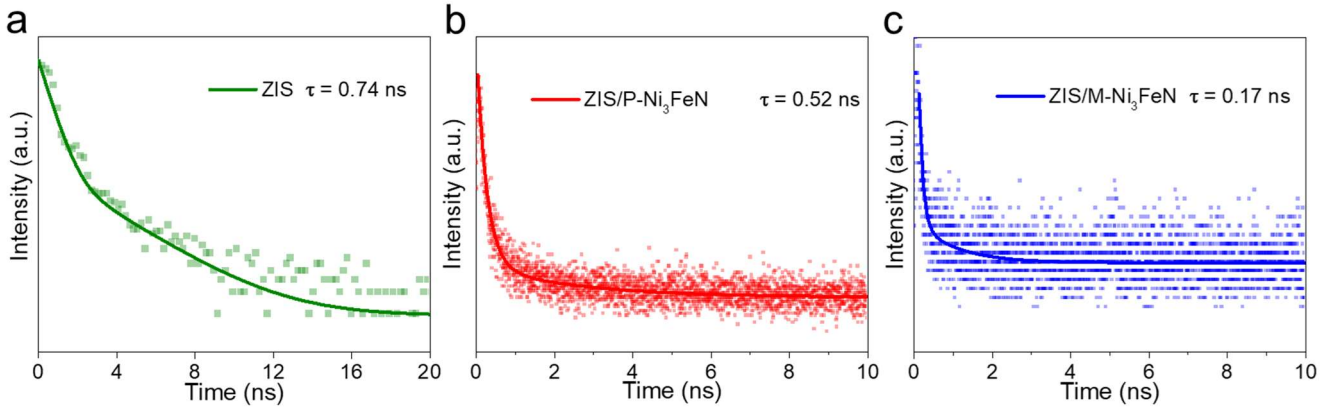

Figure S19. Transient PL spectra of ZIS, ZIS/P-Ni_3FeN and ZIS/M-Ni_3FeN composite.

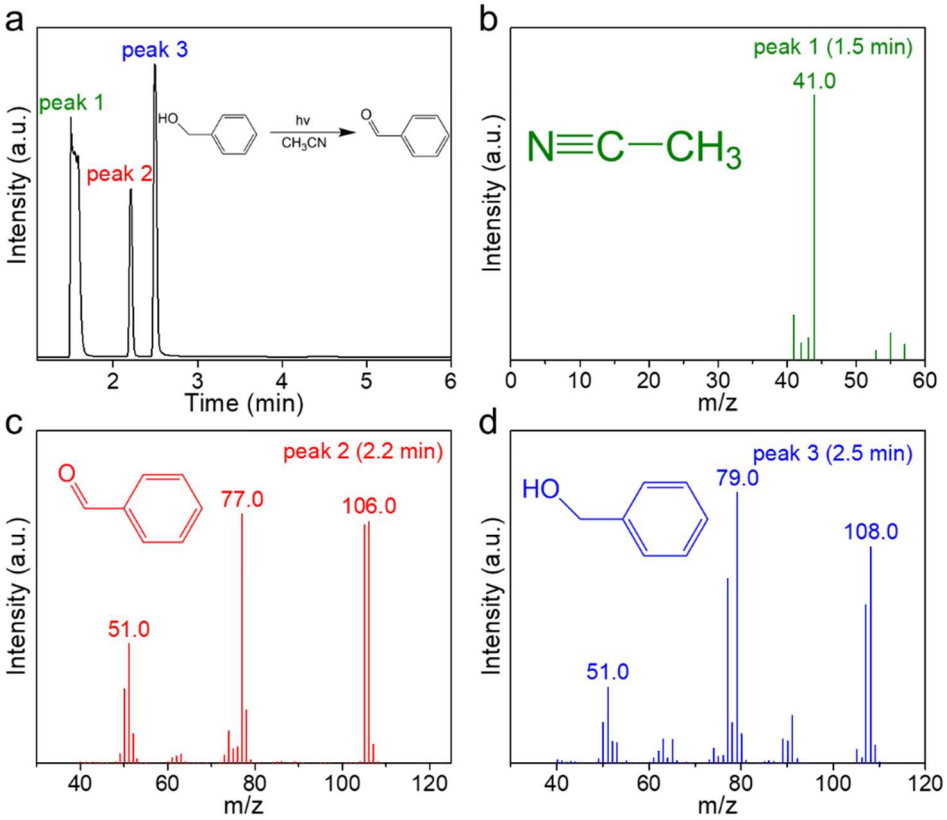

Figure S20. GC-MS spectra of the reaction solution after photocatalytic experiment. Conditions: 100 μmol benzyl alcohol, 10 mg ZIS/1.5% M-Ni_3FeN, 3 mL CH_3CN, λ > 420 nm.

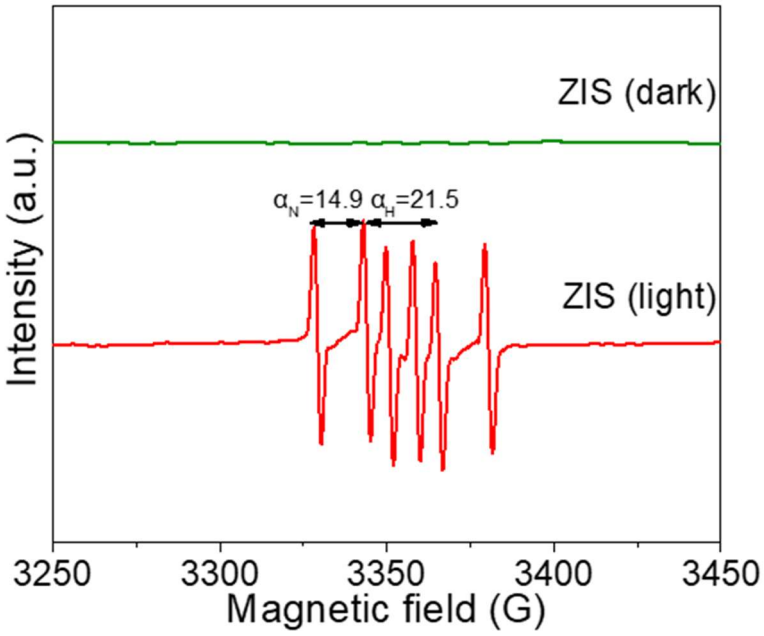

Figure S21. EPR spectrum of ZIS in the presence of DMPO in BA-CH_3CN solution under an Ar atmosphere.

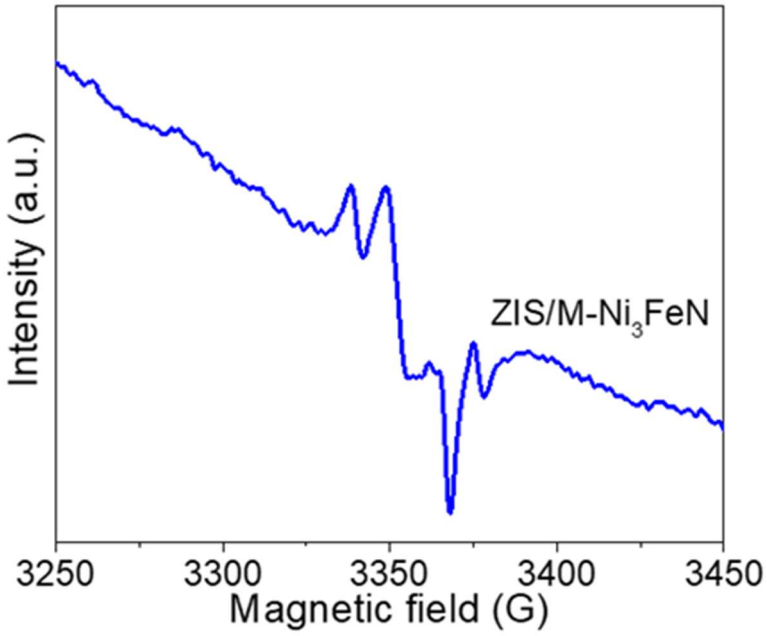

Figure S22. EPR spectrum of ZIS/M-Ni_3FeN composite in the presence of DMPO in BA-CH_3CN solution under an Ar atmosphere.

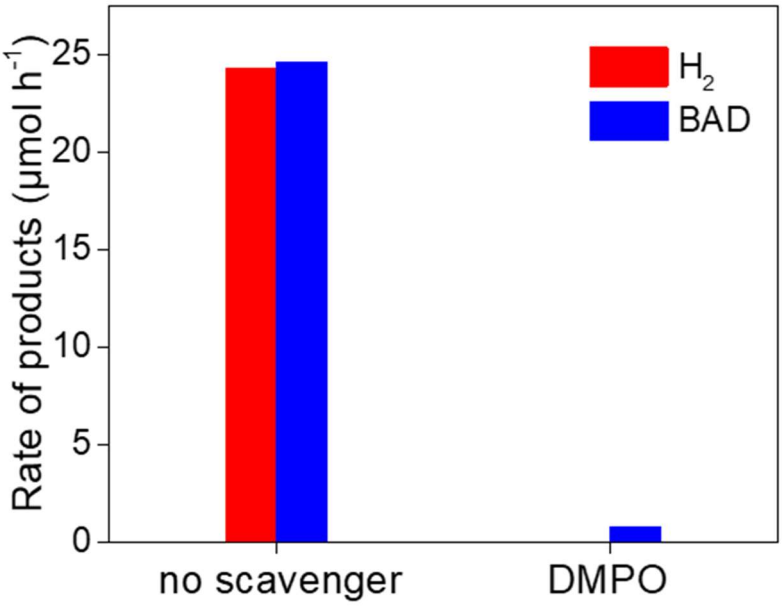

Figure S23. The effect of DMPO on the photocatalytic performance of H_2 evolution and BAD generation over ZIS/1.5% M-Ni_3FeN composite.

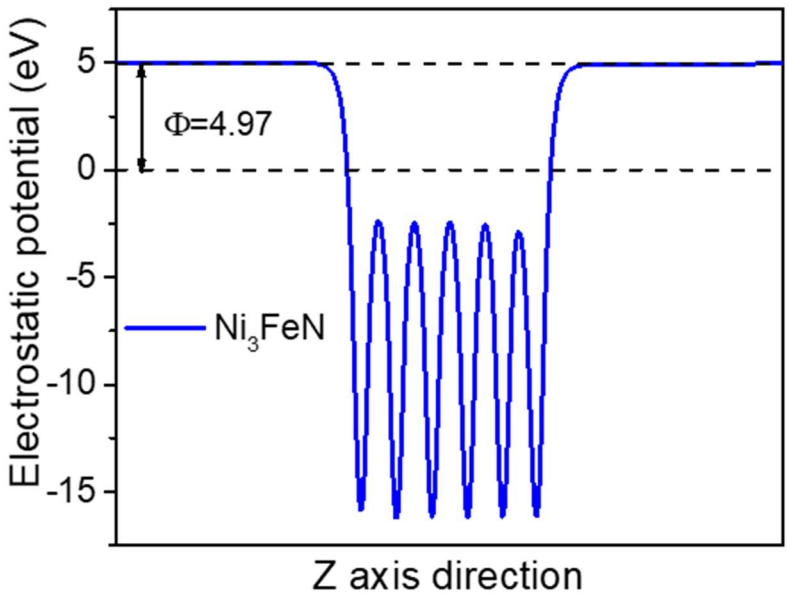

Figure S24. Work function of Ni_3FeN.

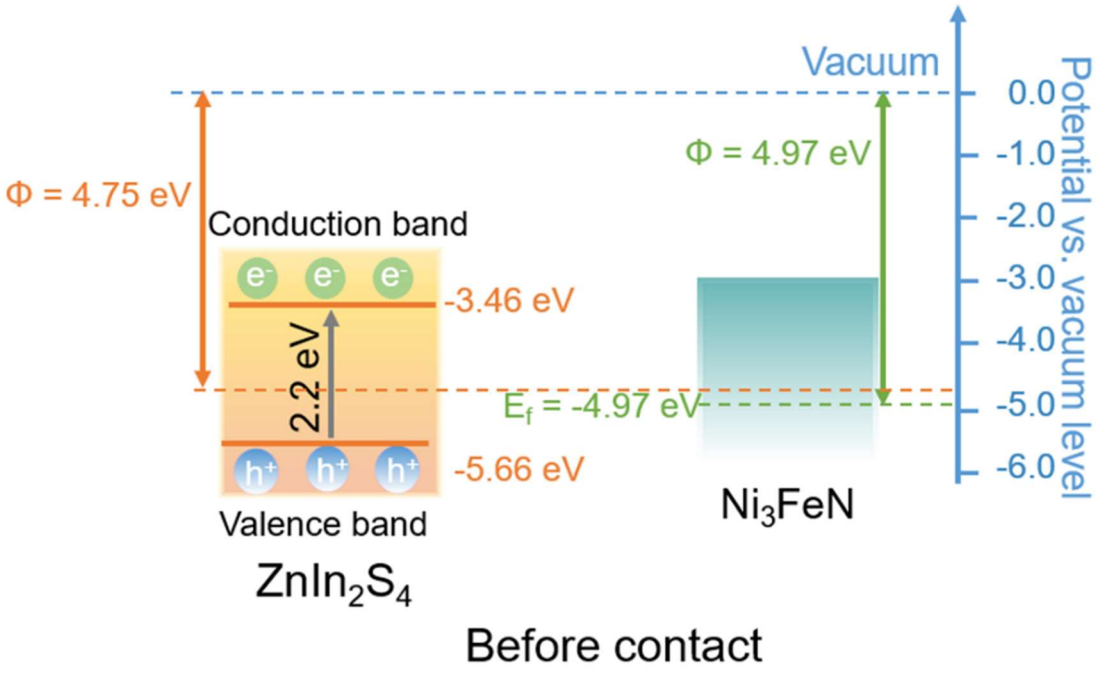

Figure S25. Energy band diagram of ZIS and Ni_3FeN before contact.

Table 1. Physicochemical Properties of Bare ZIS, ZIS/P-Ni_3FeN and ZIS/M-Ni_3FeN

Samples	S_{BET} ($m^2 g^{-1}$)	Total pore volume ($cm^3 g^{-1}$)	Mean pore diameter (nm)
ZIS	11.59	0.04	14.24
ZIS/P-Ni_3FeN	27.39	0.08	12.16
ZIS/M-Ni_3FeN	35.34	0.08	9.51

Table 2. Comparison of Performance towards Photocatalytic Coupled Selective Alcohol Oxidation and H_2 Evolution between $ZnIn_2S_4/Ni_3FeN$ and Some Recently Developed Photocatalysts

Photocatalyst	Solvent	Light source	Reaction	Selectivity (%)	H_2 (μmol g^{-1} h^{-1})	Ref.
$ZnIn_2S_4/Ni_3FeN$	CH_3CN	λ > 420 nm	BA to BAD	99	2427.9	This work
ZnS-Ni_xS_y	H_2O	λ > 200 nm	BA to BAD	90.5	2943	(1)
Pt-g-C_3N_4	H_2O	λ > 400 nm	BA to BAD	90	255	(2)
$ZnIn_2S_4/CeO_2$	CH_3CN	AM 1.5G	BA to BAD	96	1496.6	(3)
CdS(ZB)/CdS (WZ)/Ni-BTC	H_2O	λ > 420 nm	BA to BAD	90.2	2891	(4)
Pd/HNb_3O_8-H_2	H_2O	Xe lamp	BA to BAD	99	3170	(5)
VN-UP-CN	H_2O	λ > 420 nm	BA to BAD	98	196.08	(6)
W_{SA}-CN-PUNS	H_2O	λ > 420 nm	BA to BAD	93.6	298.7	(7)
$MoS_2/ZnIn_2S_4$	H_2O	λ > 420 nm	BA to BAD	-	3880	(8)
$WO_3/ZnIn_2S_4$	H_2O	UV-vis	BA to BAD	94.8	4280	(9)
Co-$ZnIn_2S_4$	H_2O	λ > 420 nm	BA to BAD	-	2823.7	(10)
CdS/MIL-53(Fe)	CH_3CN	λ > 420 nm	BA to BAD	99	2334	(11)
O-$ZnIn_2S_4/TiO_{2-x}$	H_2O	λ > 420 nm	BA to BAD	-	2584.9	(12)

REFERENCES

(1) Hao, H.; Zhang, L.; Wang, W.; Qiao, S.; Liu, X. Photocatalytic hydrogen evolution coupled with efficient selective benzaldehyde production from benzyl alcohol aqueous solution over ZnS-Ni_xS_y composites. *ACS Sustain. Chem. Eng.* **2019**, 7, 10501-10508.

(2) Li, F.; Wang, Y.; Du, J.; Zhu, Y.; Xu, C.; Sun, L. Simultaneous oxidation of alcohols and hydrogen evolution in a hybrid system under visible light irradiation. *Appl. Catal. B: Environ.* **2018**, 225, 258-263.

(3) Jiang, C.; Wang, H.; Wang, Y.; Ji, H. All solid-state Z-scheme $CeO_2/ZnIn_2S_4$ hybrid for the photocatalytic selective oxidation of aromatic alcohols coupled with hydrogen evolution. *Appl. Catal. B: Environ.* **2020**, 277, 119235.

(4) Zhang, Y.; Liu, Z.; Guo, C.; Chen, T.; Guo, C.; Lu, Y.; Wang, J. CdS (ZB)/CdS (WZ)/Ni-BTC photocatalytic selective oxidation of benzyl alcohol to benzaldehyde coupled with hydrogen evolution. *Appl. Surf. Sci.* **2022**, 571, 151284.

(5) Li, X.; Wang, T.; Zheng, Z.; Yang, Q.; Li, C.; Li, B. Pd modified defective HNb_3O_8 with dual active sites for photocatalytic coproduction of hydrogen fuel and value-added chemicals. *Appl. Catal. B: Environ.* **2021**, 296, 120381.

(6) Liu, X.; Zhang, Q.; Cui, Z.; Ma, F.; Guo, Y.; Wang, Z.; Liu, Y.; Zheng, Z.; Cheng, H.; Dai, Y.; Huang, B.; Wang, P. Morphology and defects design in g-C_3N_4 for efficient and simultaneous visible-light photocatalytic hydrogen production and selective oxidation of benzyl alcohol. *Int. J. Hydrogen Energy* **2022**, 47, 18738-18747.

(7) Zhang, F.; Zhang, J.; Wang, H.; Li, J.; Liu, H.; Jin, X.; Wang, X.; Zhang, G. Single tungsten atom steered band-gap engineering for graphitic carbon nitride ultrathin nanosheets boosts visible-light photocatalytic H_2 evolution. *Chem. Eng. J.* **2021**, 424, 130004.

(8) Chen, Z.-H.; Li, Y.-H.; Qi, M.-Y.; Tang, Z.-R.; Xu, Y.-J. Benzyl alcohol oxidation and hydrogen generation over $MoS_2/ZnIn_2S_4$ composite photocatalyst. *Res. Chem. Intermed.* **2022**, 48, 1-12.

(9) Li, Y.-H.; Qi, M.-Y.; Tang, Z.-R.; Xu, Y.-J. Coupling organic synthesis and hydrogen evolution over composite $WO_3/ZnIn_2S_4$ Z-scheme photocatalyst. *J. Phys. Chem. C* **2022**, 126, 1872-1880.

(10) Xue, J.; Liu, H.; Zeng, S.; Feng, Y.; Zhang, Y.; Zhu, Y.; Cheng, M.; Zhang, H.; Shi, L.; Zhang, G. Bifunctional cobalt-doped $ZnIn_2S_4$ hierarchical nanotubes endow noble-metal cocatalyst-free photocatalytic H_2 production coupled with benzyl alcohol oxidation. *Sol. RRL* **2022**, 6, 2101042.

(11) Li, P.; Yan, X.; Gao, S.; Cao, R. Boosting photocatalytic hydrogen production coupled with benzyl alcohol oxidation over CdS/metal-organic framework composites. *Chem. Eng. J.* **2021**, 421, 129870.

(12) Liu, J.; Wan, J.; Liu, L.; Yang, W.; Low, J.; Gao, X.; Fu, F. Synergistic effect of oxygen defect and doping engineering on S-scheme O-$ZnIn_2S_4/TiO_{2-x}$ heterojunction for effective photocatalytic hydrogen production by water reduction coupled with oxidative dehydrogenation. *Chem. Eng. J.* **2022**, 430, 133125.